JOURNAL OF MATERIALS SCIENCE 30 (1995) 4049–4058

Diamond deposition on fine vapour grown carbon filament

JYH-MING TING
Applied Sciences, Inc., Cedarville, OH 45314 USA

A fine carbon filament has been used as substrate in a microwave plasma enhanced chemical vapour deposition (MPECVD) process. The carbon filaments were severely etched to form carbon dusts which then served as nucleation seeds. Polycrystalline diamond coatings on the carbon dust and the diamond dust, which was used during the sonication pre-treatment, were obtained at temperatures below 1000 °C. A mini-explosion that formed a 120-μm diamond sphere occurred at a temperature of 950 °C. As the processing temperature further increased, several explosions occurred to form protrusions, including glassy carbon spheres with volumes greater than 22 mm^3, and thick glassy carbon coatings, at an average rate as high as 270 μm per 17 h, on the entire surface. These thick coatings occurred on the untreated surface of a Si coupon, which was used to support the carbon filaments. The explosion has been explained to be as a result of energy absorption from the microwave and plasma.

1. Introduction

Low pressure synthesis of diamond involving the use of hydrocarbon and hydrogen mixtures occurs when the gaseous mixtures are activated by d.c. or r.f. arc discharge [1, 2], microwave energy [3–5], d.c. glow discharge [6] or hot filaments [7, 8]. The synthesis can also be performed by using combustion reactions between oxygen and some hydrocarbons [9]. Although the mechanism of diamond synthesis is not well established, it is recognized that diamond can be deposited from the vapour phase on diverse substrate materials. However, relatively little research has been reported where carbon materials (exclusive of diamond) have been used as substrate wafers. Studies [10,11] have indicated that formation of diamond occurred on the edge of graphene planes, as well as on scratches left by diamond abrasion. Another study [12] also reported that, using highly oriented pyrolytic fibre (HOPG) as a substrate, diamond nucleated interiorly on the basal plane, better on very highly disordered carbon surface, and best on a lightly polished basal plane surface or prism plane surface. In any event, however, diamond nucleation on a carbon substrate wafer was found to be difficult. However, when a carbon fibre known as a vapour-grown carbon fibre was used as substrate, diamond formation was found to be relatively easy [13–15]. In this paper, we have further investigated deposition of diamond on a fine vapour-grown carbon filament. Although the principle of producing the carbon filament and vapour grown carbon fibre (VGCF) are similar, distinctive results have been observed.

2. Experimental procedure

The carbon filaments used in this study were prepared in our laboratory [16]. This type of filament has a diameter of 0.2 μm and a length near 100 μm. The d.c. conductivity of as-grown filament is at least $1 \times 10^5\ \Omega^{-1}\,m^{-1}$. Carbon filaments were first sonicated in a dilute aqueous solution containing distilled water and a small amount of high-purity diamond dust (0–2 μm in diameter) and then in distilled water. After this pre-treatment, a drop containing filaments was transferred to a Si coupon to form a porous thin coverage. Filaments occupied the centre area, approximately 0.4 to 0.5 cm in diameter, of the 1×1 cm Si coupon. The Si coupon with filaments was then subjected to a 2.45 GHz microwave reactor for 17 h of deposition. During each run, the specimen was placed in a position to obtain the desired temperature, ranging from 800 to 1200 °C. The microwave power was maintained at a constant 210 W. Other processing conditions used are summarized in Table I. Specimens were characterized by scanning electron microscopy (SEM) and micro-Raman spectroscopy.

3. Results

Fig. 1 shows SEM micrographs of specimens obtained under conditions A to D. Coatings were inhomogeneous and found mainly in the centre zones

TABLE I Processing conditions used in the current study

Conditions	Gas mixture (H_2/CH_4 in sccm)	Temperature (°C)		Pressure kPa
		Initial	Final	
A	99.4/0.5	800 ± 5	800 ± 5	3.99
B	99.4/0.5	850 ± 5	845 ± 5	3.99
C	99.4/0.5	900 ± 5	905 ± 5	3.99
D	95.4/0.5	950 ± 5	950 ± 5	3.99
E	99.5/0.5	1000 ± 5	1200 ± 5	3.99
F	99.9/0.1	1000 ± 5	1200 ± 5	3.99

0022–2461

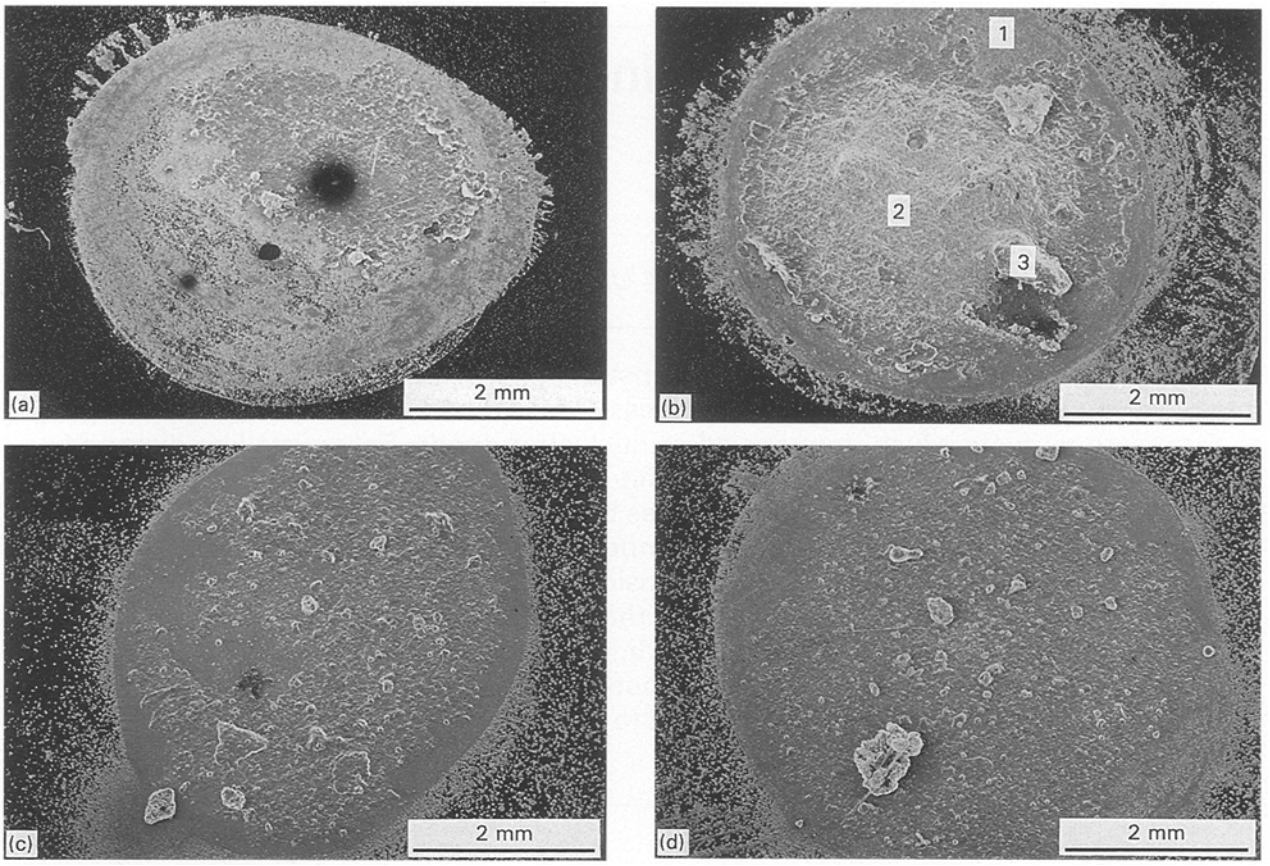

Figure 1 SEM micrographs of specimens obtained under conditions A to D. Coatings were inhomogeneous and found mainly in the centre zones (defined by the broken line) which were originally covered by the carbon filament. The arrows define different morphologies as categorized in the text.

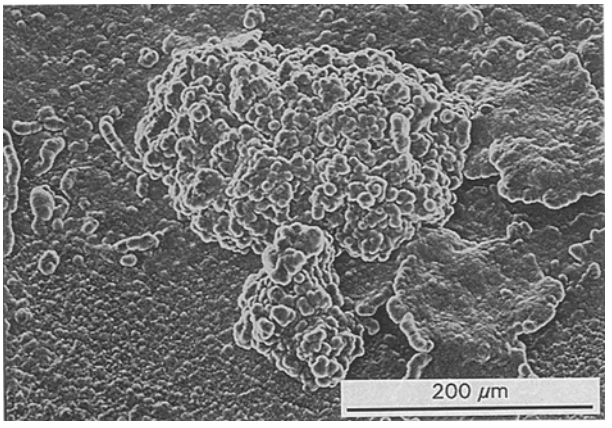

Figure 2 Colloidal aggregate-like and flake-like agglomerates are commonly found on the specimens shown in Fig. 1.

which were originally covered by carbon filaments. There are in general three common morphologies found in the centre zones: "planar" surface morphology as Region 1 in Fig. 1(b), "island-like" morphology as Region 2 in Fig. 1(b), and agglomerate-like morphology as Region 3 in Fig. 1(b). It appears that as the processing temperature increased, heavier coatings were obtained such that the island-like and agglomerate-like morphologies became more pronounced. The agglomerates are in the shape of either colloidal aggregate or flake as shown in Fig. 2. Both colloidal aggregates and flakes have the same ball-like structure (Fig. 3(a)) which consists of faceted crystals that are smaller than those found in the planar and island regions (Fig. 3(b)). In the regions outside the above described centre zones, diamond nucleation was also

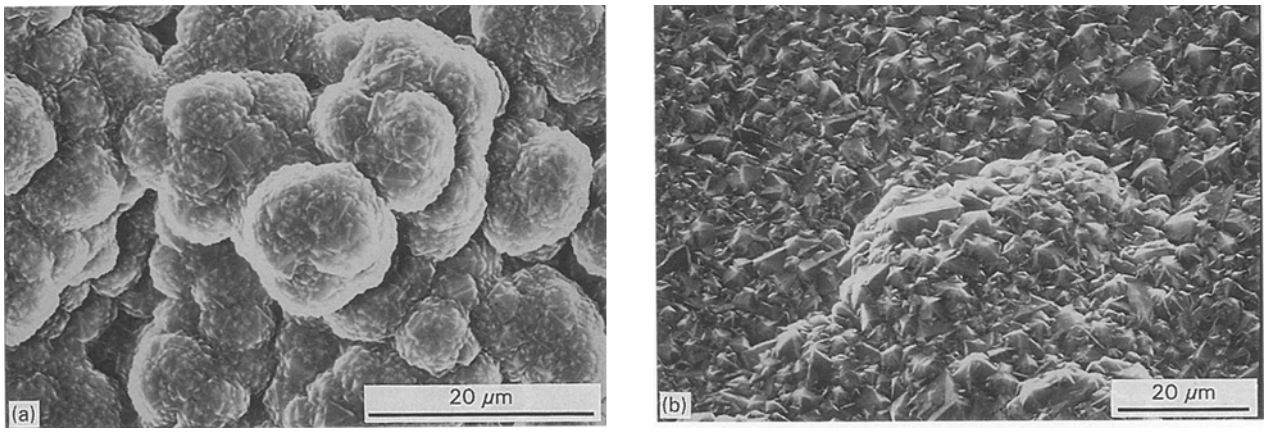

Figure 3 Morphologies of (a) colloidal aggregates and flakes and (b) planar and island-like regions. Colloidal aggregates and flakes have the same ball-like structure which consists of faceted crystals that are smaller than those found in the planar and island regions.

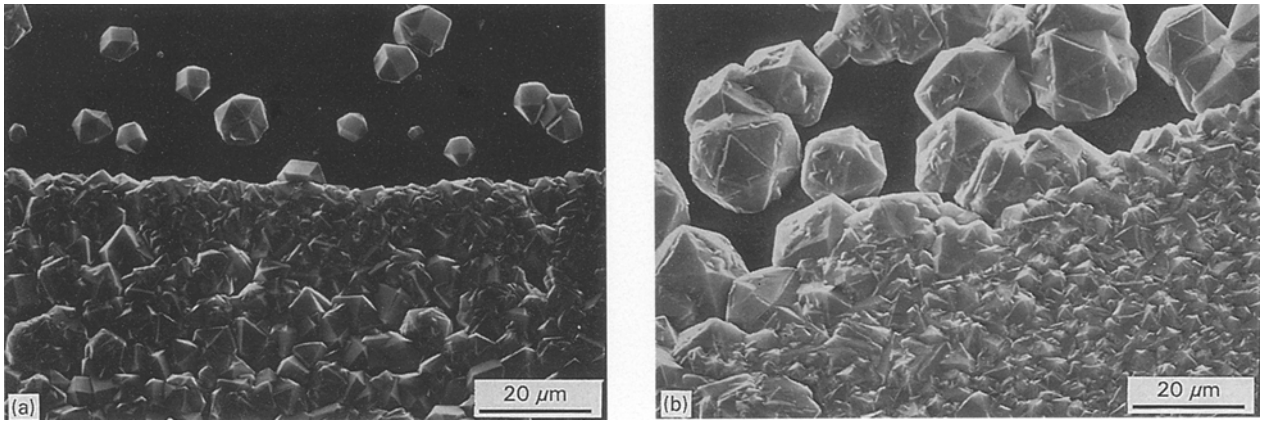

Figure 4 Larger crystal sizes with more defects are found on a specimen obtained at a higher temperature. The processing temperatures were (a) 800 °C and (b) 900 °C.

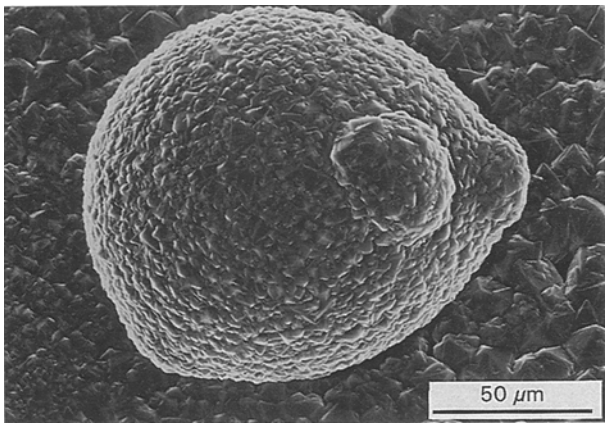

Figure 5 A sphere with two lumps was observed on a specimen processed under condition D.

observed. Higher nucleation densities are seen in areas closer to the centre zone and at higher temperatures as shown in Figs 1 and 4. Fig. 4 also demonstrates that larger crystals are found on specimens obtained at a higher temperature.

Two distinct features were also found on specimen prepared under condition D (temperature = 950 °C). A sphere with two lumps was observed as shown in Fig. 5. The diameter of the sphere is about 120 μm and the lumps, 25 to 35 μm. These two lumps on its surface may be a result of secondary nucleation [17]. The second feature, as shown in Fig. 6, is the fibrous morphology found mostly in the region outside the centre zone and less on the agglomerates. Fig. 6(b) and (c) show that the microstructure of the faceted "fibres" found in both places are the same. Also the crystal sizes are similar to that of the agglomerates.

When the temperature was 1000 °C, even larger sphere-like morphology was observed. Fig. 7(a) and (b) show, respectively, a top view and a side view of specimen obtained under condition E. A large "hot balloon" is seen in the centre of the specimen. The diameter of the hot balloon is about 3.5 mm. The density of the balloon was determined to be 1.5 $g\,cm^{-3}$, approximately. The surface morphology of balloon appears to consist of non-faceted "fibres" (Fig. 8(a)) and a porous "matrix" (Fig. 8(b)). The microstructure of both the fibre and the matrix are

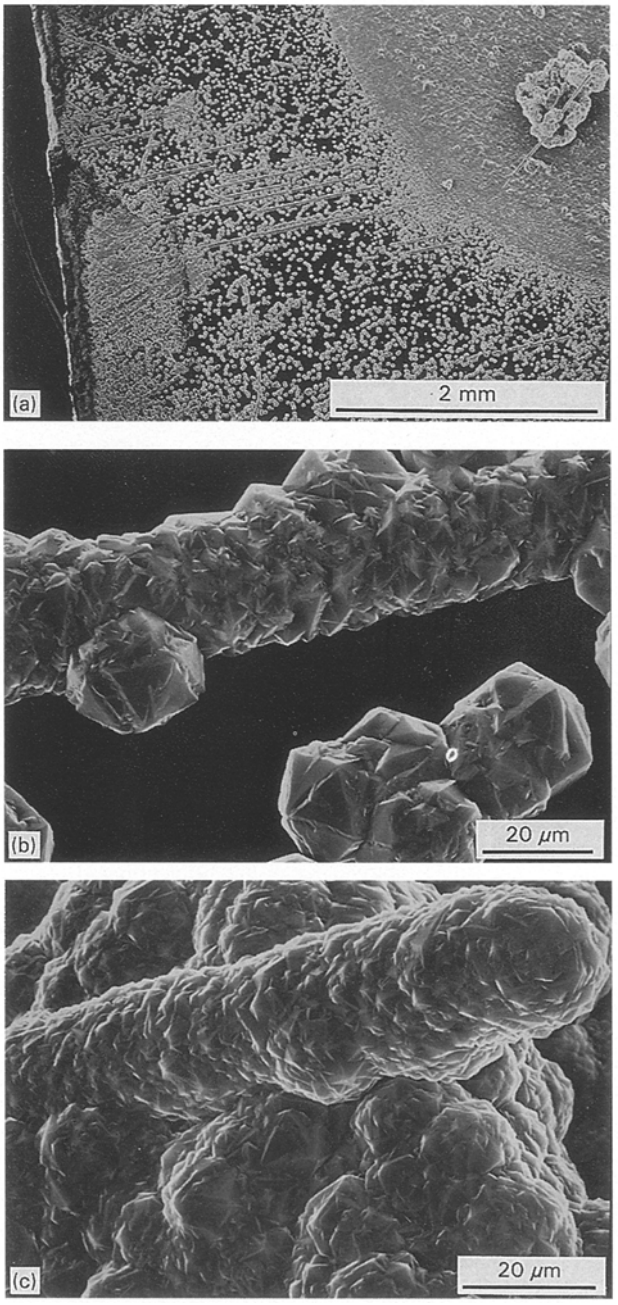

Figure 6 Fibrous morphology found (a) mostly in the area outside the centre zone and less on the aggregates. The microstructure of the "faceted fibres" found (b) outside the centre zone and (c) on the aggregates is the same.

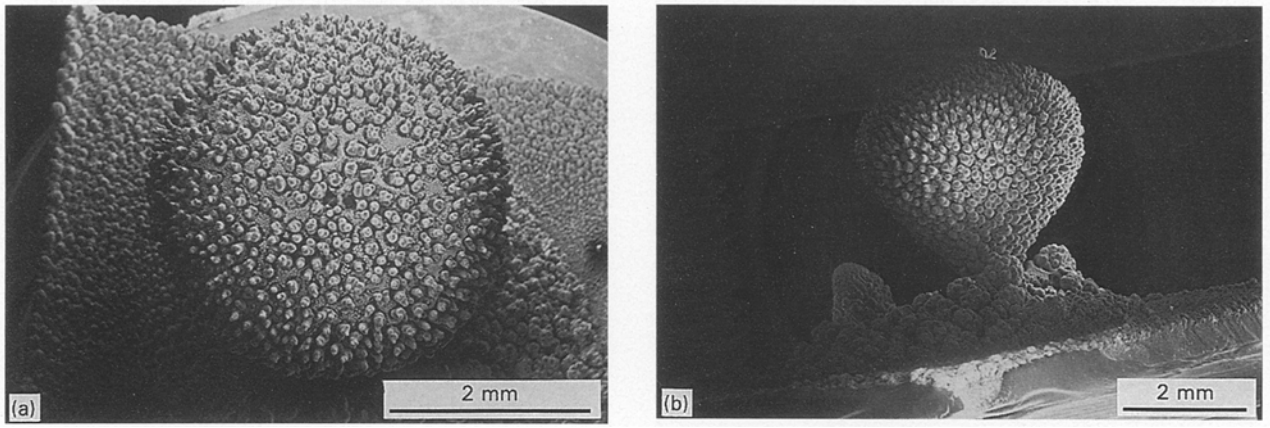

Figure 7 SEM micrographs showing (a) a top view and (b) a side view of a specimen obtained under condition E.

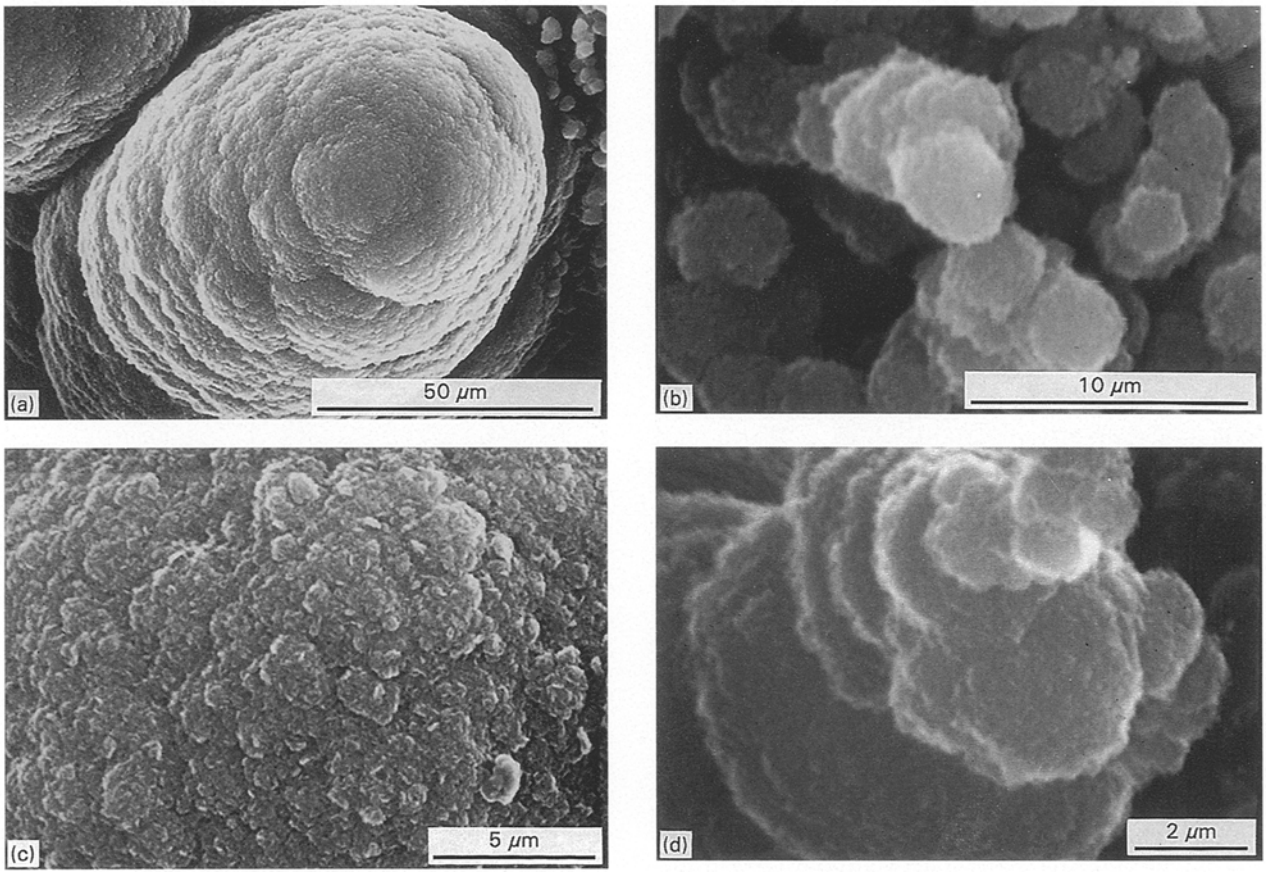

Figure 8 The surface morphology of hot balloon appears to consist of (a) non-faceted fibres mixed with (b) a porous "matrix". The microstructure of both (c) the fibre and (d) the matrix are similar.

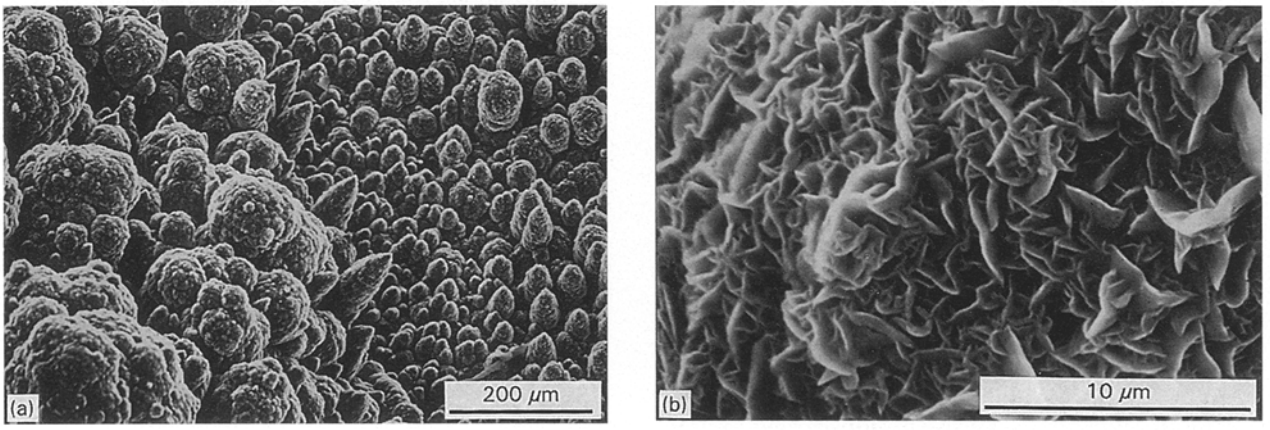

Figure 9 (a) Surrounding the hot balloon are hills of agglomerate-like coatings consisting of colloidal aggregate-like and corn-shaped morphologies. (b) Both regions exhibit flake-like microstructure.

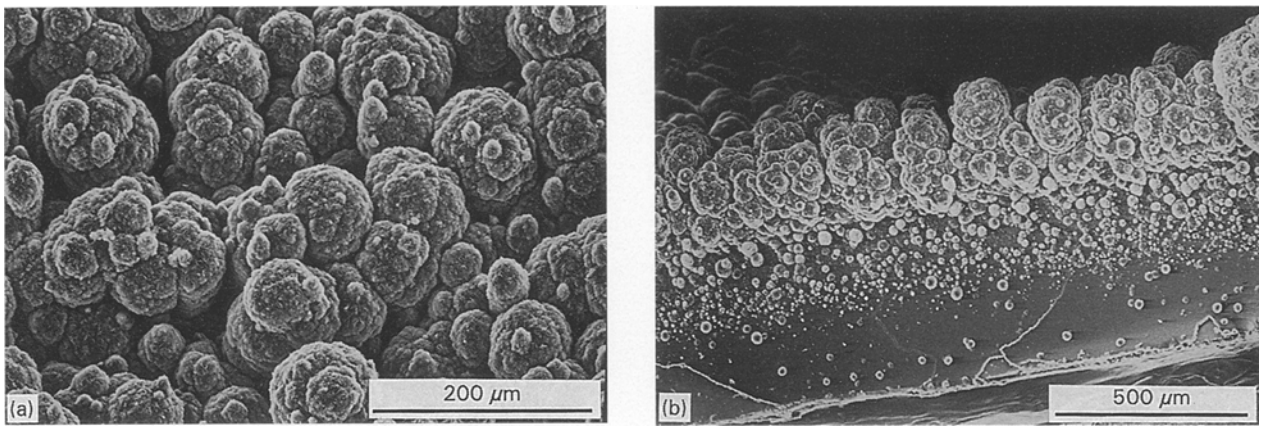

Figure 10 Found away from the hill region are "planar" coatings consisting of colloidal aggregates, which also exhibit a flake-like microstructure: (a) top view and (b) side view.

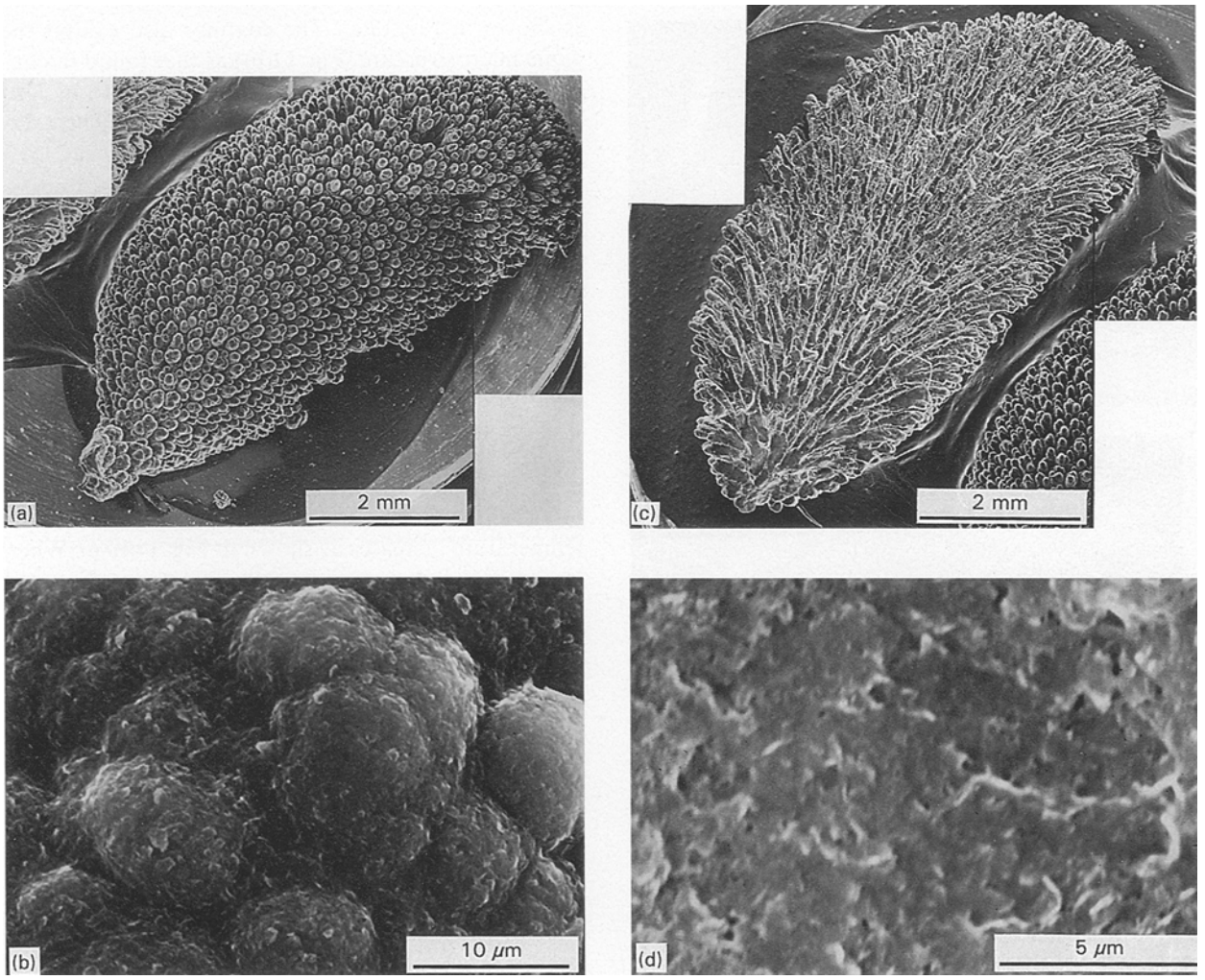

Figure 11 A distorted ellipsoid was formed at the centre of a specimen processed under condition F. (a) Surface morphology, (b) microstructure of the ellipsoid, (c) morphology of as-cut surface and (d) its microstructure.

similar as shown in Figs 8(c) and (d), respectively. Surrounding the hot balloon are hills of agglomerate-like coatings. The coatings consist of colloidal-aggregate-like and cone-shaped morphologies (Fig. 9(a)), both of which exhibit flake-like microstructure (Fig. 9(b)). Found away from this region are "planar" coatings consisting of colloidal aggregates, which also exhibit a flake-like microstructure. This is shown in Fig. 10 for both top view and side view of the planar region. The coating thickness of the planar region was determined to be about 270 μm.

For specimen processed under condition F, similar morphology was found. A distorted ellipsoid was formed at the centre of specimen. The density is also 1.5 $g\,cm^{-3}$, approximately. The surface morphology is shown in Fig. 11a. The ellipsoid was cut into two parts and the as-cut surface morphology is shown in Fig. 11c. Both surfaces exhibit microstructure, as

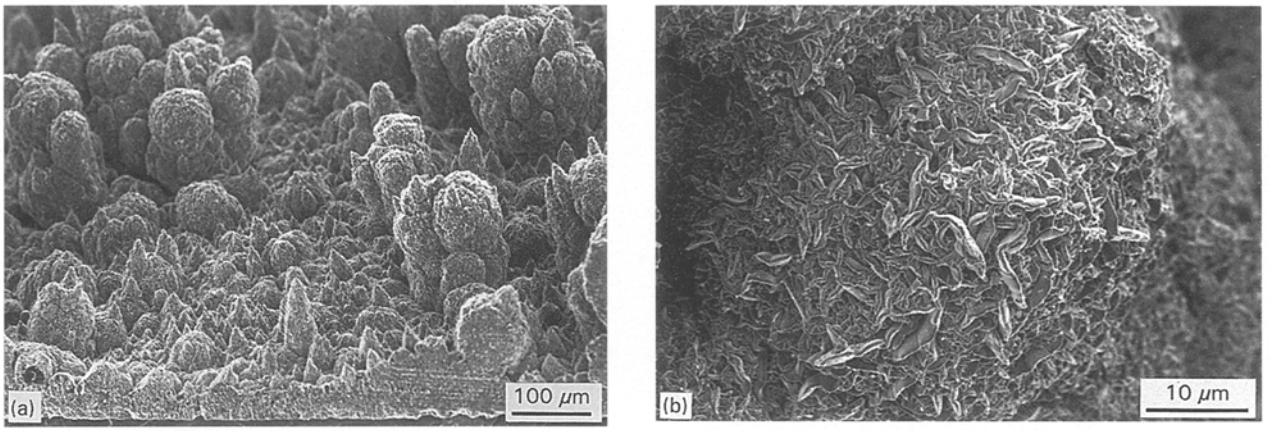

Figure 12 (a) Surrounding the ellipsoid are hills of agglomerate-like coatings. (b) The coatings also exhibit the same microstructure as that found in condition E.

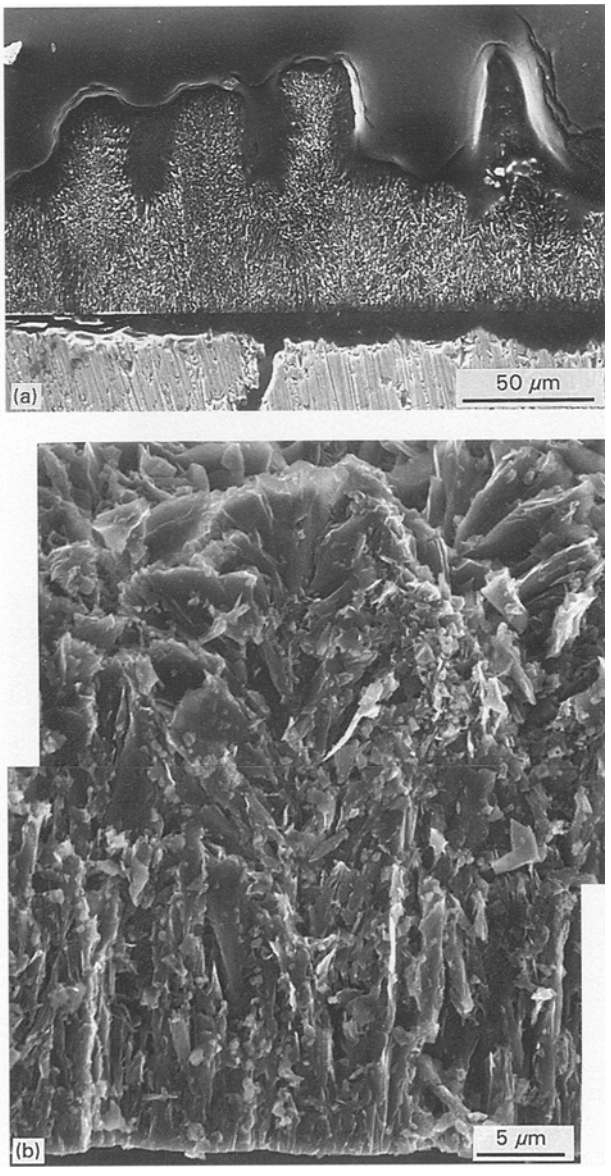

Figure 13 Cross-sectional views, at different magnifications, of the coatings shown in Fig. 12(a). (a) × 500 (b) × 3500.

shown in Fig. 11(b) and (d), resembles that of the hot balloon (Fig. 8(c)).

Surrounding the ellipsoid, hills of agglomerate-like coatings were found as in the previous condition. This is shown in Fig. 12(a). The coatings also exhibit the same microstructure (Fig. 12(b)) as that found in condition E. The cross-section of the coatings was also examined. Fig. 13 shows such an example. The average coating thickness was estimated to be at least 50 μm.

Raman spectroscopy analysis was performed to analyse the coatings obtained. Fig. 14(a) and (b) show the Raman spectra taken from two different areas on a specimen obtained under condition A. Characteristics of diamond and graphitic inclusion can be seen in both spectra. It is seen that the diamond to graphitic inclusion ratio is higher in the planar region (Fig. 14(a)) than in the agglomerates (Fig. 14(b)). The Raman spectra of the planar region and island-like region are found to be similar. For the Raman spectra on the agglomerates, the ratio also decreases when the temperature increases as shown in Fig. 14(b–e). When the processing temperature was 1000 °C the diamond characteristic peak no longer exists. Results from Raman spectroscopy analysis on specimens obtained under conditions E and F indicate the formation of glassy carbon as shown in Fig. 15. Fig. 15(a) and (b) are the Raman spectra on the hot balloon (Fig. 7) and the coatings shown in Fig. 12.

4. Discussion

4.1. Diamond formation at temperatures less than 1000 °C

4.1.1. Diamond nucleation sites

Diamond coatings were obtained at temperatures of 800, 850, 900, and 950 °C. It is thought that diamond formation occurred mainly on two different groups of nucleation sites or seeds. They are the severely-etched carbon filaments and the diamond dust remaining after the sonication processes.

The fine carbon filaments used in this study are produced by the pyrolysis of H_2/CH_4 mixtures in the presence of iron catalytic particles less than 20 nm in diameter [16]. Depending on the concentration of CH_4 and the processing time, fine carbon filaments or carbon fibre can be obtained. Both the filament and fibre exhibit very similar microstructure with graphene

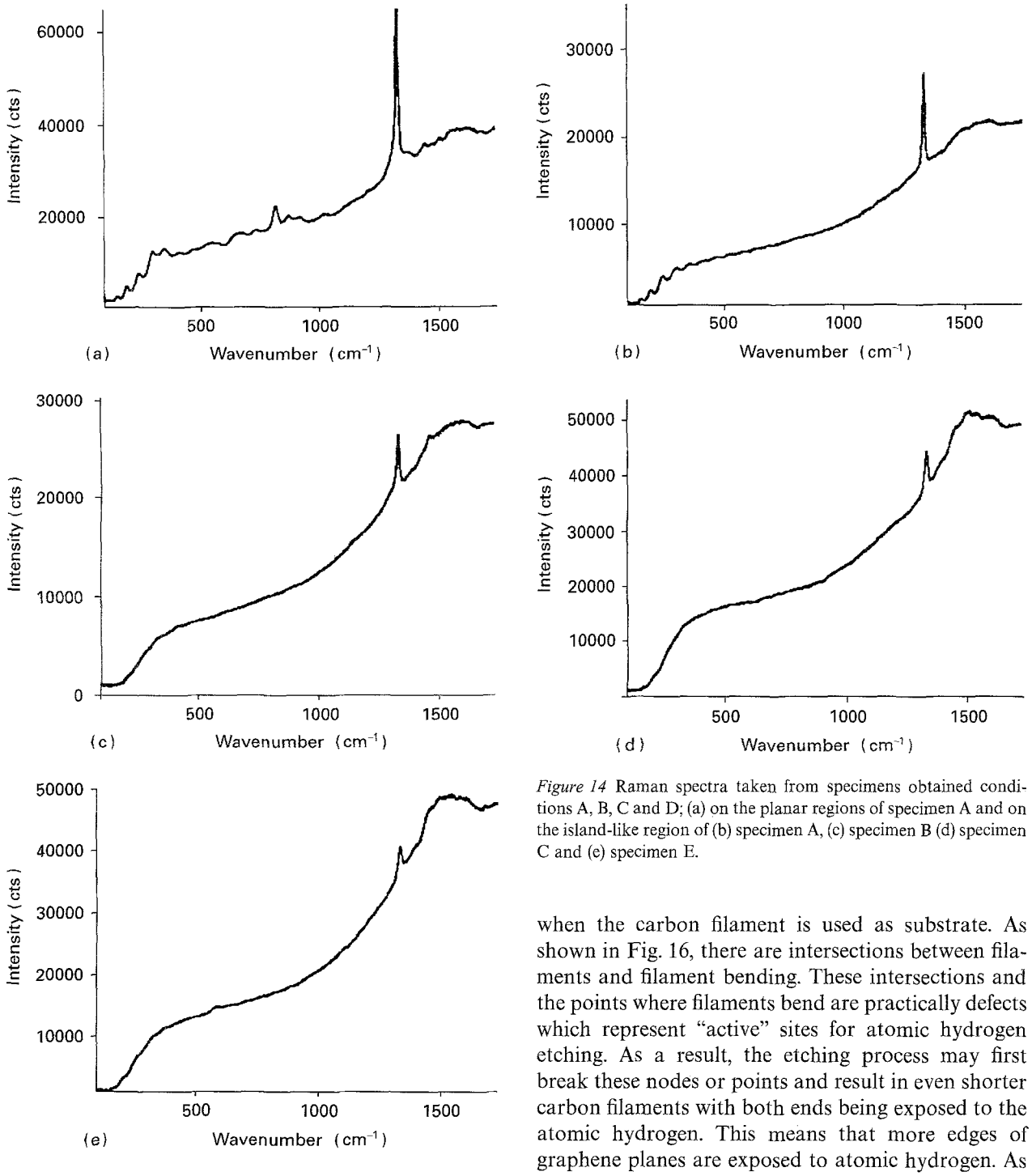

Figure 14 Raman spectra taken from specimens obtained conditions A, B, C and D; (a) on the planar regions of specimen A and on the island-like region of (b) specimen A, (c) specimen B (d) specimen C and (e) specimen E.

planes parallel to the fibre longitudinal direction and very similar properties with the filament being more graphitic. The fibre has a diameter of 5 to 7 μm and a length of 10 to 30 cm, while the filament has a diameter of 0.2 μm and a length near 100 μm. Due to the nature of its forming process, entangled carbon filaments result as shown in Fig. 16. These filaments also have very low surface energy, which is low enough to create a surface area of 1×10^7 cm^2 g^{-1} or an apparent specific volume as high as 3×10^3 cm^3 g^{-1}.

Previous studies have demonstrated the formation of high quality diamond on vapour grown carbon fibre [13–15]. After the deposition of diamond, the carbon fibre was found to be etched by atomic hydrogen as indicated by the reduction of its diameter. The atomic hydrogen etching is believed to also occur when the carbon filament is used as substrate. As shown in Fig. 16, there are intersections between filaments and filament bending. These intersections and the points where filaments bend are practically defects which represent "active" sites for atomic hydrogen etching. As a result, the etching process may first break these nodes or points and result in even shorter carbon filaments with both ends being exposed to the atomic hydrogen. This means that more edges of graphene planes are exposed to atomic hydrogen. As compared to the surface, the ends which exhibit edges of graphene planes are thought to be more viable for atomic hydrogen etching. Therefore, the etching process would cause an increase in the shorter carbon filament becoming carbon dust as atomic hydrogen etches the ends at a rate faster than etching the remaining area. Based upon the observation on coating vapour-grown carbon fibre with diamond, this etching process is necessary and also serves as an incubation period. During the incubation, a kinetic competition between the etching rate and the formation rate of hydrogen "dangling bonds" takes place [13]. In the case of using carbon filaments as substrate, the incubation may last to the point where most of the carbon filaments have become carbon dust. After the incubation, diamond can therefore successfully nucleate and grow on the carbon dust. Occasionally, there are whiskers left, as shown in Fig. 6. A similar mechanism

was reported on diamond nucleation on Si coated with sub-micron carbon film [18]. The high nucleation density observed was attributed to the formation of a porous ultra-thin residual carbon film due to atomic hydrogen etching.

In addition to the carbon dust, diamond dust may also serve as nucleation sites. It is well known that diamond nucleation on Si can be enhanced by polishing the Si surface with diamond abrasive prior to deposition. The mechanism has been reported to be that, after the pre-treatment, diamond particles remain on Si and serve as nucleation sites or seeds [19, 20]. In the present study, it is believed that a small amount of diamond dust also remained on the carbon filaments, after the sonication process, and was transferred to the Si coupon. The diamond dust then served as diamond nucleation sites or seeds for subsequent diamond growth.

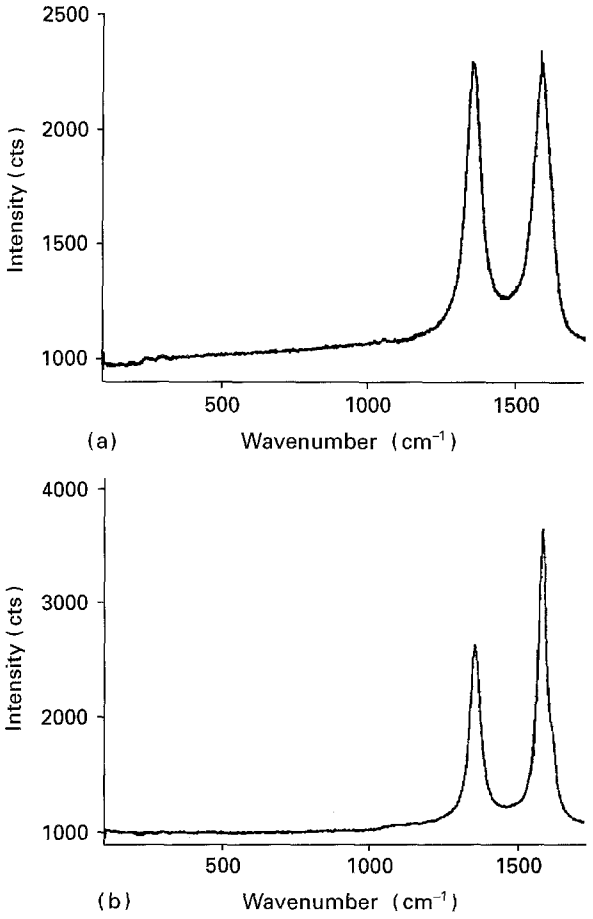

Figure 15 Raman spectra on (a) the balloon shown in Fig. 7 and (b) the coatings shown in Fig. 12.

4.1.2. The distribution of nucleation sites

The morphology of diamond coatings can generally be categorized into three groups: planar surface morphology, island-like morphologies, and agglomerate-like morphology. The crystal sizes in the planar region and the island-like region are similar and larger than those of the agglomerates. The formation of such morphologies and crystals with different sizes is thought to be related to the difference in nucleation site and its distribution.

As mentioned previously, a small amount of diamond dust remained on the carbon filaments. Due to the bulky and entangled nature, the filaments might form a loose three-dimensional network on the surface of Si. The bulky, entangled carbon filaments were then etched by atomic hydrogen at a rate much faster than that of etching diamond dust [21], leaving the resulting carbon dust and the diamond dust on Si. The etching broke the three-dimensional network of the carbon filaments to form piles of carbon dust. In the areas where the carbon filaments were completely etched, the diamond dust dropped to the surface of the Si coupon. As the deposition process continued, diamond formation occurred on piles of carbon dust which survived the etching or incubation, leading to the development of agglomerate-like morphology. On the other hand, the remaining diamond dust might be distributed on the Si in a way that heavier dust occurred close to the centre of the Si coupon. This led to the development of planar and island-like morphologies as diamond formation took place on the diamond dust.

It is noted that the crystals are smaller in the agglomerate-like region than in the planar and island-like regions. This is attributed to the time available for diamond formation, the difference in the size of nucleation seed, and the difference in the density of nucleation seeds. The formation of diamond on the carbon dust requires an incubation [13–15] while the

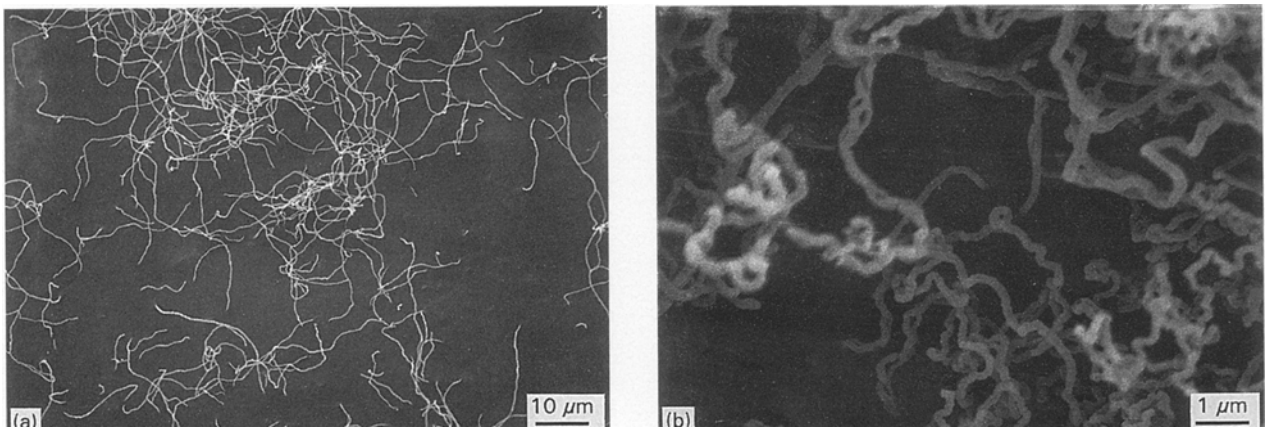

Figure 16 SEM micrographs of the carbon filaments used in this study.

diamond dust requires no or very brief incubation [17]. As a result, the time available for diamond formation on diamond dust is longer than on carbon dust, leading to larger crystals on the diamond dust. In addition, serving as nucleation seeds, the dimensions of the diamond dust (0 to 2 μm in diameter) are apparently larger than that of carbon dust, which again leads to larger crystals on the diamond dust. Furthermore, the density of diamond dust is believed to be lower than that of the carbon dust. This allows diamond crystals to grow for a longer time before collision of crystals occurs. Previous work indicates that, using the same pre-treatment method and plasma conditions, diamond crystals grown on Si are at least five times larger than those grown on vapour-grown carbon fibre [22].

4.2. Diamond formation on the region outside the centre zone

As shown in Figs 1 and 4, diamond deposition also occurred on the regions outside the centre zones. These regions were not pre-treated by any method. The nucleation density of diamond on such a region is estimated to be approximately 5×10^5 cm^{-2}, obtained under condition A. This is higher than that normally obtained on un-treated Si surface [23]. As the temperature increased, the nucleation density increased. In addition, as shown in Fig. 6(a), fibrous morphology was found in this region as temperature increased to 950°C. The crystal sizes on these fibres are similar to those of the agglomerates and smaller than those of the planar and island-like regions in the centre zone, while the crystal sizes on the rest of the region are similar to those of the planar and island-like regions. Furthermore, higher nucleation densities are seen in the areas closer to the centre zones. These findings suggest that a very small amount of the diamond dust and traces of carbon filaments may be pushed away from the centre zones through the interaction between them and the microwave/plasma. This interaction becomes more pronounced when temperature increases, as suggested by higher nucleation densities at higher temperatures. As the temperature increases further, it is believed that explosion occurs. A mini-explosion that yielded a 120-μm sphere has been observed, as shown in Fig. 5.

4.3. Microwave energized explosion

Microwave energy has been used in processing of synthetic diamond [13–15], sintering of ceramic materials [24, 25], and joining of ceramic materials [26]. In these applications, microwave energy can be used as a direct and/or indirect source for heating. For direct heating, as in a sintering process, a material is heated through the interaction between microwaves and the material [27, 28]. For indirect heating, reaction gas is ionized by microwave energy to form plasma which interacts with material to provide heating. In the case of diamond synthesis with no substrate heater, a substrate is heated primarily by the energy released from the recombination of hydrogen atoms and, to a lesser degree, by microwave energy, as most of the substrate materials absorb limited or little microwave energy when a conventional 2.45 GHz microwave source is used.

However, carbon materials (excluding diamond) can be easily heated to 1000 °C at a power level near 1 kW (2.45 GHz microwave) [29]. The skin depth [30], defined as the depth at which the electric field drops to $1/e = 0.368$ of the surface value, of carbon with a d.c. conductivity of 0.1 Ω^{-1} m^{-1} is in the order of 1×10^1 cm when the microwave frequency is 2.45 GHz. The skin depth is inversely proportional to the square root of d.c. conductivity. As a result, very graphitic carbon materials, which exhibit higher d.c. conductivities, can be heated at a similar heating efficiency provided that the dimensions are properly reduced.

For the carbon filament used in this study, the skin depth was estimated to be only in the order of 1×10^2 μm at a microwave frequency of 2.45 GHz. However, it is two orders of magnitude higher than the diameter of the carbon filament and in the same order of magnitude as that of filament length. This leads to the absorption of a substantial amount of microwave energy by the carbon. This also accounts for the higher temperatures observed on the carbon filaments than that on Si in the beginning of the deposition. In addition to the microwave energy, the energy released from the recombination of hydrogen atoms is also absorbed by the carbon. As a result, the total energy absorbed by the carbon filaments, coupled with the high surface area, generated the explosion. The explosion resulted in the formation of deposit on the entire Si coupon surface and protrusion on the centre region of Si. It is not known when the explosion occurred exactly. However, a possible mechanism is proposed below.

As the deposition starts, the etching process also takes place. During the incubation or etching, several mini-explosions occur to cover various locations of the Si surface with debris (i.e. carbon dust, diamond dust, or short carbon filaments). The mini-explosion may last until the entire Si coupon surface is covered by the seeds. As the process continues, deposition occurs at the end of the incubation. Heavier coatings occur in the centre zone as it has more nucleation seeds and a higher seed density. Coatings also occur on the debris as shown in Fig. 13. As noted previously, the average coating thickness can be as thick as 270 μm when the methane concentration is 0.5% or 50 μm when the methane concentration is 0.1%. Some coatings exhibit cone-shaped morphology (Fig. 12(a)) as found in other CVD processes. As the process further continues, the absorption of energy also continues. This explains that the temperature raised from 1000 °C at the beginning to 1200 °C at the end of experiment. As enough energy is accumulated, the major explosion occurs in the centre zone which leads to the formation of protrusions. The explosion also brings small particles to the surfaces of the hot balloon and the distorted ellipsoid, due to the low mass, to form the porous matrix (Fig. 7(a)). Fig. 11(c) shows

a pattern such that fibrous coatings explode to form a distorted ellipsoid. The major explosion may occur near the end of experiment since the coated fibres have a fairly uniform diameter which is also similar to the sizes of the aggregates. However, the secondary nucleation found in Fig. 5 suggests that after the major explosion, there is time that allows deposition to occur before the conclusion of the experiment.

Finally, the above discussion on the interaction between microwave and material does not include the contribution from the magnetic field vector of the microwave. This is due to the fact that the magnetic field vector induces microwave losses in magnetic materials and the carbon filaments used are not magnetic.

5. Conclusion

Diamond formation can occur on graphitic carbon such as the carbon filament used in this study. The formation occurs after an incubation during which a kinetic competition between the atomic hydrogen etching rate and the formation rate of hydrogen "dangling bonds" takes place. Due to the unique properties of the carbon filament, explosion may occur as enough energy is absorbed from the microwave and plasma. The explosion leads to the formation of protrusions and thick coatings. The protrusions include glassy carbon spheres with diameters larger than 3 mm and volumes greater than 22 mm^3. The thick glassy carbon coatings on the untreated surface of a Si coupon was found to grow at an average rate of 270 μm per 17 h when the methane concentration was 0.5% or 50 μm per 17 h when the methane concentration was 0.1%. These findings suggest that under proper conditions, fast rate deposition of polycrystalline diamond and formation of polycrystalline diamond beads are viable by using the carbon filaments as nucleation seeds.

Acknowledgements

Part of this work is supported by an NSF under Grant No. III-9261081. Some of the SEM analysis was performed by J.A. Makeeff at Jeol USA, Inc., Peabody, MA.

References

1. N. OHTAKE, H. TAKURA, Y. KURIYAMA, Y. MASHIMO and M. YOSHIKAWA, Proceedings of 1st International Symposium on Diamond and Diamond-Like Films (The Electrochemical Society, 1989).
2. C. LI, Y.C. LAU, and S.L. GIRSHICK, in Proceedings of 2nd International Symposium on Diamond Materials (The Electrochemical Society, 1991).
3. M. KAMO, Y. SATO, S. MATSUMOTO and N. SETAKA, *J. Cryst. Growth* **62** (1983) 642.
4. R. MEILUNAS, M.S. WONG, K.C. SHENG and R.P.H. CHANG, *Appl. Phys. Lett.* **54** (1989) 2204.
5. M. KAMO and Y. SATO, in Proceedings of 2nd International Symposium on Diamond Materials (The Electrochemical Society, 1991).
6. M. PETERS, J.M. PINNEO, L.S. PLANO, K.V. RAVI, V. VERSTEEG and S. YOKOTA, *SPIE Proc.* **877** (1988) 79.
7. S. MATSUMOTO, Y. SATO, M. KAMO and N. SETAKA, *Jpn. J. Appl. Phys.* **21** (1982) L183.1
8. W.A. YARBROUGH, K. TANKALA and T. DEBROY, *J. Mater. Res.* **7** (1992) 379.
9. Y. HIROSE, S. AMANUMA, N. OKADA and K. KOMAKI, in Proceedings of 1st International Symposium on Diamond and Diamond Like Films (Electrochemical Society, 1989).
10. J. ANGUS, in "Diamond Films '91", Nice, France, September, 1991 (Elsevier, Switzerland).
11. T. SUZUKI, Z. LI, A. ARGOITA and P. PIROUZ, in Wayne State University Third Annual Diamond Technology Workshop, March, 1992.
12. J.J. DUBRAY, C.G. PANTANO and W.A. YARBROUGH, *J. Appl. Phys.* **72** (1992) 3136.
13. J.-M. TING and M.L. LAKE, *J. Mater. Res.* **9** (1994) 636.
14. Idem., *Diamond Rel. Mater.* **3** (1994) 1243.
15. M.L. LAKE, J.-M. TING and J.F. PHILLIPS, Jr., *Surface Coat. Technol.* **62** (1993) 367.
16. J.-M. TING and M.L. LAKE, in Proceedings of the International Conference on Processing, Fabrication, and Applications Advanced Composites, Long Beach, CA, 1993 (ASM Internat. Materials Park, OH).
17. J. SINGH and M. VELLAIKAL, *J. Appl. Phys.* **73** (1993) 15.
18. Z. FENG, K. KOMVPOULOS, I.G. BROWN and D.B. BOGY, *Ibid.* **74** (1993) 2841.
19. H. MAEDA, S. IKARI, T. OKUBO, K. KUSAKABE and S. MOROOKA, *J. Mater. Sci.* **28** (1993) 129.
20. C.-M NIU, G. TSAGAROPOULOS, J. BAGLIO, K. DWIGHT and A. WOLD, *J. Solid State Chem.* **91** (1991) 47.
21. N. SEKADA, in Proceedings of 10th International Conference on CVD, edited by G.W. Cullen and J. Blocher, Jr (The Electrochemical Society, 1987).
22. J.-M. TING, Final Report, NSF Grant No. III-9261081, September, 1993.
23. P.N. BARNES and R.L.C. WU, *Appl. Phys. Lett.* **62** (1993) 4.
24. A.J. BERTEAUD and J.C. BADOT, *J. Microwave Power* **11** (1976) 315.
25. D.L. JOHNSON, *Ceram. Trans.* **21** (1991) 17.
26. T.T. MEEK and R.D. BLAKE, *J. Mater. Sci. Lett.* **5** (1986) 270.
27. W.H. SUTTON, *Ceram. Bull.* **68** (1989) 376.
28. Idem., *Proc. Mater. Res. Soc.* **124** (1988) 7.
29. R.E. NEWNHAM, S.J. JANG, M. XU and F. JONES, *Ceram. Trans.* **21** (1991) 51.

Received 23 August 1994
and accepted 21 February 1995